

Numerical Simulation of Radiation-Induced Chemical Segregation and Phase Transformation in a Binary System

Efraín Hernández-Rivera^{1,2}, Veena Tikare¹ and Lumin Wang²

Abstract: We present the development of a hybrid Monte Carlo-phase field model that is able to simulate radiation induced chemical segregation and the corresponding phase transformation and nano-structure evolution. Under irradiation by a low-energy ion beam, defects (vacancies) are created and accumulate. In a binary crystalline material, AB, studied in this work, these defects are of the two types A and B and diffuse at different rates. These differential diffusivities are sufficient driving mechanisms for the formation of chemically distinct regions with accompany changes in phases and nano-structure. In this work, we present a model that can simulate these changes by treating the differential diffusion of the vacancies of the two components.

Keywords: chemical segregation, Monte Carlo, phase field, phase transformation.

1 Introduction

Ion irradiation increases the number of point defects past the point of saturation, causing unique microstructural changes. It is well known that ion-irradiation can lead to chemical separation in a multi-component system, which is essentially an effect driven by the difference in diffusivities of interstitials and vacancies of the different components. This is better known as radiation induced segregation (RIS). This radiation effect has been observed in a wide variety of materials including binary [Okamoto and Rehn (1979); Wiedersich, Okamoto and Lam (1979)] and multi-component [Bruemmer, Simonen, Scott, Andresen, Was and Nelson (1999)] systems. Some of these materials also show interesting microstructural features forming like nano-cones [Le Roy, Barthel, Brun, Lelarge and Sondergard (2009)] and nano-fibrous structures [Perez-Bergquist, Sun, Wang and Zhang (2009)].

¹ Advanced Nuclear Energy Programs, Sandia National Laboratories, Albuquerque, NM, USA.

² Nuclear Engineering and Radiological Sciences, University of Michigan, Ann Arbor, MI, USA.

Diffusion in irradiated materials has been widely studied [Was (2007)], mostly for metallic multi-component systems under in-reactor radiation conditions where the material is subjected to high energy ion fluxes. RIS has also been observed in materials subjected to low- to mid-ion energy irradiation. However, under these conditions, sputtering theory says that the chemical segregation observed is due to preferential sputtering of the different component near the surface region rather than differential diffusion. Sputtering theory has also been employed to explain the formation surface nano-structures, like nano-cones [Le Roy, Barthel, Brun, Lelarge and Sondergard (2009); Perez-Bergquist, Li, Zhang and Wang (2010)], nano-ripples [Bradley and Harper (1988); Wei, Lian, Boatner, Wang and Ewing (2009)] and quantum dots [Wei, Lian, Lu and Wang (2008)]. Madi, Anzenberg, Ludwig Jr. and Aziz (2011), proposed another mechanism to explain the formation of these surface nano-structures; they suggested mass redistribution lead to nano-structure formation. In this work, we develop a model to simulate differential diffusion and apply it to determine if differential diffusion in a two-component, multiphase system is sufficient to observe RIS and phase transformation. We use numerical simulations to study compositional evolution, phase transformation and microstructural changes of a binary system under irradiation.

2 Model Development

We studied a multi-phased binary (AB) system with thermodynamic characteristics described in Fig. 1. We use a model that couples continuum and statistical methods, which we refer to as the hybrid model, to simulate the generation of vacancy defects due to irradiation, diffusion of components A and B , phase transformation and microstructural evolution. The model is based on the hybrid Potts-phase field model developed by Homer, Tikare and Holm (2013), but is further developed to simulate radiation damage and its effects on diffusion.

2.1 Microstructural and Composition Representation

We use continuous fields to represent the chemical composition and vacancy density, and discrete fields to represent the phases. The simulation space is digitized into 2D squares, called sites, where the discrete field in each square describes its phase state and the continuous fields have digital values at that grid point. The starting microstructure consists of an AB solid in contact with vacuum, called void. The concentration of vacancies is zero (as the equilibrium vacancies is very low) and the chemical composition is $C_A = C_B = 0.5$ at all sites. Periodic boundary conditions are used in the x -direction only, hence, in effect, the solid is a semi-infinite solid with an irradiated surface in contact with a vacuum.

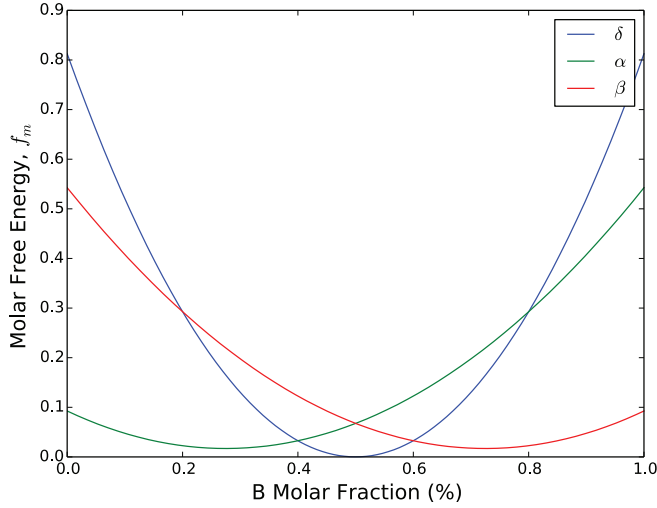


Figure 1: Isothermal chemical free energy curves for the two-component, three-phase system being modeled.

2.2 Radiation Damage

Radiation damage and its accumulation are modeled as radiation-induced vacancies and the increase in the vacancy concentration with continued radiation. The calculation of radiation damage is a three-step process: calculate the probability of collision event taking place at a given depth due to radiation by an ion beam; determine the number of defects created by the collision cascade; and compute the number of surviving defects.

The first two steps are described by Gaussian distribution probabilities. Each one has characteristics that precisely describe them and is obtained from a TRIM calculation [Ziegler, Ziegler and Biersack (2008)]. From these distributions, we are able to calculate the number of vacancy defects that are generated during the collision cascade stage. The defects that contribute to diffusion and RIS are the ones that survive the quenching stage when many of the defects heal by recombining. To determine the number of surviving defects, we use the method employed by Hobler, Simionescu, Palmetshofer, Tain and Stinger (1995)

$$\eta_s(E_T) = \eta_{TRIM}(E_T) f_{rec}(1 - 2p_{ref}) \quad (1)$$

where $\eta_{TRIM}(E_T)$ is the number of Frenkel pairs created due to the energy transferred (E_T) as calculated from TRIM, f_{rec} is the fraction of η_{TRIM} that did not recombine within the collision cascade and p_{ref} is the probability that a newly created

defect will recombine with a pre-existing defect. We should note that for simplicity, we only consider the *net* creation of vacancy defects. In this manner, the vacancy concentration at each site increases continuously throughout irradiation.

A more detailed description of the radiation damage calculation can be found in Hernández–Rivera, Tikare and Wang (2013)

2.3 Chemical and Vacancy Evolution

The RIS model developed by Wiedersich, Okamoto and Lam (1979) couples point defect kinetic equations to track the evolution of these defects. In this hybrid model, we model this field by use of an *adapted* Cahn–Hilliard equation

$$\frac{\partial C_v}{\partial t} = \eta_s(\Delta t) + \nabla \cdot \left(M_v \nabla \cdot \left[\frac{\partial f_v}{\partial C_v} - \kappa_v \nabla^2 C_v \right] \right) \quad (2)$$

where $\eta_s(\Delta t)$ is the concentration of surviving defects during irradiation time interval Δt 1 is added to the change in concentration due to diffusion, M_v is the mobility of the vacancies, κ_v is an interfacial energy constant and f_v is the vacancy bulk free energy defined as by the regular solution equation

$$f_v = \frac{1}{\Omega} (E_v^f C_v + k_B T [C_v \ln(C_v) + (1 - C_v) \ln(1 - C_v)]) \quad (3)$$

where Ω is the unit site volume and E_v^f is the vacancy formation energy. For the evolution of the chemical components, we use an approach similar to the one given by Wiedersich, Okamoto and Lam (1979), and outlined in Was (2007). The different point defect fluxes through an *AB* system are

$$\begin{aligned} J_i &= J_i^A + J_i^B \\ -J_v &= J_v^A + J_v^B \end{aligned} \quad (4)$$

where J_i^A is the flux of defect through the site of *A* component. Since we are considering a binary system and using Fick's first law, Eq. 4 could be simplified for a single component

$$C_A + C_B = 1 \rightarrow \nabla C_A = -\nabla C_B \quad (5)$$

Now, using Fick's second law and setting the net flux to include diffusion due to chemical gradients and through the defect mechanisms just discussed, we have

$$\frac{\partial C_B}{\partial t} = \nabla \cdot (D_B \nabla C_B - D_v^B \nabla C_v) \quad (6)$$

where the first term is the flux due to a chemical gradient, and the second term is the flux through the vacancy and interstitial defects, respectively. We have omitted the

diffusion due to interstitial mobility since we are assuming a net increase of zero interstitials due to irradiation. Lastly, we model differential diffusion by assigning a much faster diffusion coefficient to the B than to the A component when diffusion occurs through the vacancy hopping mechanism, i.e., $D_v^A < D_v^B$.

We use the standard approach for nondimensionalizing the Cahn-Hilliard equation by defining a set of normalizing parameters to non-dimensionalize Eqs. 2 and 6. The normalizing parameters are energy

$$E_n = k_B T \quad (7)$$

and length

$$l = \sqrt{\frac{\kappa_v}{k_B T}} \quad (8)$$

where interfacial energy constant, κ_v has units of $length^2 \cdot energy$ giving l units of length. Finally, normalized time is

$$\tau = \frac{l^2}{D} = \frac{l^2}{M_v k_B T} \quad (9)$$

where the mobility, M_v , has units of $length^2 / (energy \cdot time)$ giving τ units of time. Eqs. 2 and 6 in their non-dimensional forms are obtained by applying to the corresponding quantities by normalized energy, length or time as

$$\frac{\partial C_v}{\partial \tilde{t}} = \tilde{\eta}_s(\Delta \tilde{t}) + \tilde{\nabla} \cdot \left(\tilde{M}_v \tilde{\nabla} \cdot \left[\frac{\partial \tilde{f}_v}{\partial C_v} - \tilde{\kappa}_v \tilde{\nabla}^2 C_v \right] \right) \quad (10)$$

and

$$\frac{\partial C_B}{\partial \tilde{t}} = \tilde{\nabla} \cdot (\tilde{D}_B \tilde{\nabla} C_B - \tilde{D}_v^B \tilde{\nabla} C_v) \quad (11)$$

We should point out that the radiation damage equations were generated as to obtain distributions that yield an ion range of $\sim 50nm$. As for each pixel, we treat them as cubes of length $L \approx 2nm$. For temporal dimension, the radiation event per MCS were determined using the beam *flux density* of $\sim 10^{15} ion / (cm^2 \cdot s)$, which translates to $1 MCS \approx 0.1875s$.

2.4 Phase Transformations

The phase state at each individual pixel is described by a discretized integer value. In our system we consider three phases, shown in Fig. 1: δ (AB), α (A-rich) and β

(B-rich). To incorporate radiation damage, the free energy of the δ phase includes a vacancy term

$$f_{\delta} = f_{\delta}^{bulk} + f_v + E_{int} \quad (12)$$

where f_{δ}^{bulk} is the chemical free energy shown in Fig. 1, f_v is given in Eq. 3 and E_{int} is the Potts interfacial energy given by

$$E_{int} = \sum_{n=1}^N \gamma_n \delta_{spin(i),spin(n)} \quad (13)$$

where γ_n is a scaling coefficient of the interfacial energy and $\delta_{spin(i),spin(n)}$ is the Kronecker delta.

Two mechanisms are driving the system towards a phase nucleation event: chemical segregation and increased vacancy concentration. As collision events due to irradiation create vacancies and these diffuse through the system, the chemical components segregate leading to lower energy configurations with α and β phases. As previously stated, radiation damage is modeled as the vacancies introduced to the system with a commensurate increase in the free energy. Therefore, as vacancies are accumulated, the δ phase becomes increasingly unstable, shown in Fig. 2. Once formed, these nuclei can grow and coalesce with a transition probability given by

$$P_{\text{phase change}} = \begin{cases} 1, & \Delta f_B^{bulk} \leq 0 \\ 0, & \Delta f_B^{bulk} > 0 \end{cases} \quad (14)$$

where Δf_B^{bulk} is the change in the chemical bulk free energy calculated using Eq. 12 for the phase transformation of that site. For a phase nucleation event we compare the difference in the chemical bulk free energies of the different phases. If the new phase has a lower free energy, then the phase change is accepted. These nuclei can grow by the standard grain growth algorithm [Holm and Battaile (2001)], if the sites neighboring the nucleus reduces its total free energy given by Eq. 12.

2.5 Phenomenological Approach

In Hernández-Rivera, Tikare and Wang (2013), the concentration gradient was used as the driving force to evolve the microstructure. It was noticed that even though chemical segregation was achieved, the microstructure generated was not representative of the system's physical or thermodynamic characteristics. In order to have a proper thermodynamic description of the component segregation and phase transformation of the multi-phase system, the chemical potential must be used as the driving force, so Eq. 11 becomes

$$\frac{\partial C_B}{\partial \tilde{t}} = \tilde{\nabla} \cdot (\tilde{D}_B \tilde{\nabla} \mu_B - \tilde{D}_v^B \tilde{\nabla} \mu_v) \quad (15)$$

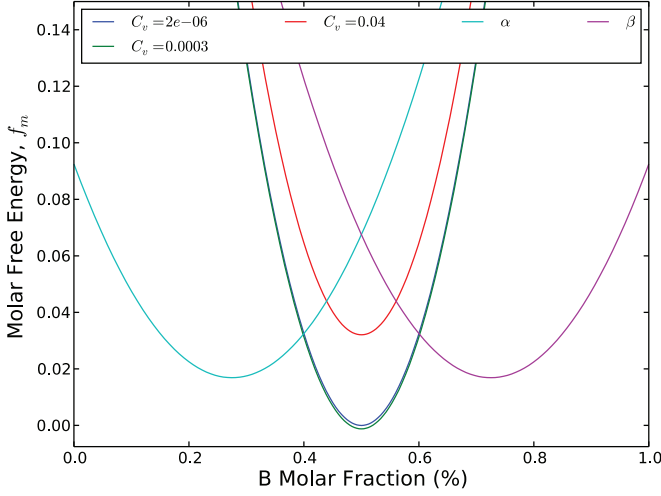


Figure 2: Evolution of the system's thermodynamics as radiation damage accumulates.

to properly evolve the microstructure by leading the system to a thermodynamic quasi-equilibrium.

Phasefield models use the simplified definition of chemical potential, $m = \partial f / \partial c$ as they use a continuous function for free energy f with minima corresponding to the stable phases and compositions. However, simulation of the binary AB with a variable free energy f_δ corresponding to the density of irradiation defects, the full definition of chemical potential is required. In this section, the implementation of the complete chemical potential is described and the results of these simulations are shown.

2.5.1 Chemical Potential Definition

When using the simplified definition of the chemical potential, our model presented very unstable solutions to the microstructural evolution. Therefore, we use the complete definition of the chemical potential for the case where two phases with two different free energy curves are in equilibrium, as defined by the *Common Tangent Construction* [Lupis (1983)], shown in Fig. 3. This approach defines the chemical potential as

$$\mu_B = f_B + (1 - C_B) \cdot \frac{\partial f_B}{\partial C_B} \tag{16}$$

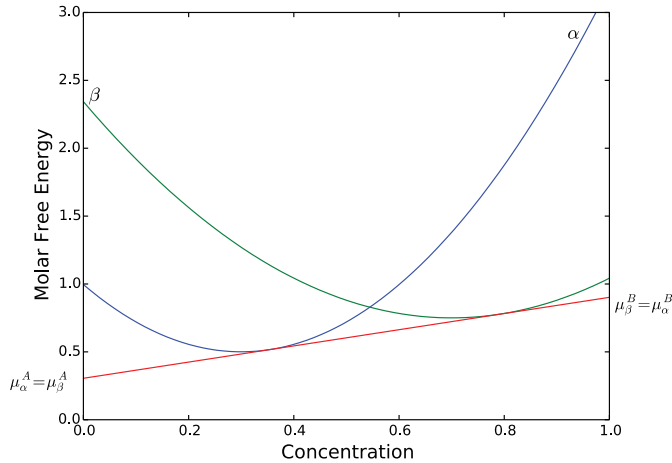


Figure 3: Graphical representation of the chemical potential as defined by the Method of Intercepts-Common Tangent Construction approach.

where f is the sum of the chemical free energy (f_B^{bulk}) and the interfacial energy (E_{int}). This approach enables us to properly describe the microstructural evolution where the two phases move towards equilibrium, especially in the phase interfaces. It should be noted, that to the best of our knowledge, this is the first time that this description has been used to define and apply the chemical potential in a phase field problem.

2.6 Processes Implementation

This hybrid model is able to incorporate all these processes to simultaneously simulate the microstructural evolution due to ion irradiation. The simulation proceeds as:

1. Calculate if a collision event occurs, i.e. $p_{coll} < RN$ where RN is a random number.
 - (a) If $p_{coll} < RN$, calculate number of stable defects created and locally update the vacancy concentration, η
2. For time iterations, during each Monte Carlo step (MCS), the compositional evolution equations are solved 100 times.
 - (a) Locally solve the adapted Cahn–Hilliard equation, Eq. 10, and the chemical evolution equation, Eq. 15

- (b) Globally update the chemical and vacancy concentrations
- (c) Update time, $t = t + \Delta t_{\text{phase field}}$ where $\Delta t \gg \Delta t_{\text{phase field}}$

3 Results and Analysis

To test the model, we simulate irradiation of a stoichiometric AB material consisting of a single grain of the δ phase. The ion irradiation beam has a distribution peaking close to the center of the material, as shown in Fig. 4. We have a sketch showing the radiation-induced defect center of the simulation space and how it evolves as the vacancies diffuse away from the defect rich region. As the defects diffuse away from the center, small regions become chemically segregated, which leads to the nucleation of distinct phases. A Gaussian-like vacancy concentration distribution as shown in Fig. 5(c) is generated. The differential vacancy diffusivity leads to chemical segregation. As shown in Fig. 5, initially we get enrichment of component A around the radiation distribution peaking region. As A is enriched in this high vacancy density region, nucleation of the α -phase is achieved. Due to periodic boundary conditions and a uniform segregation induced enrichment of A along the horizontal direction, this phase grows quickly. This in turn, leads to an enrichment of B at the α -phase interface since the B component is being driven away from the nucleated phase. Eventually, we see nucleation of the β -phase, which is driven to a higher concentration, i.e. B enrichment.

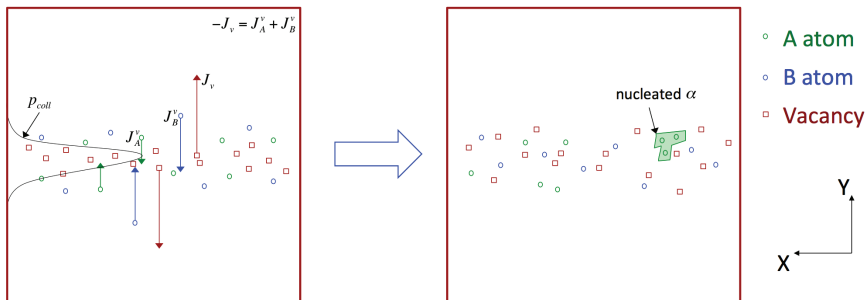


Figure 4: Schematic of the simulation space, a 2D binary compound, AB, is being irradiated with an ion beam with collision probability as shown in the left. The collision probability peaks at the center as shown, with the largest concentration of vacancies also occurring there. Vacancies diffuse to regions of lower concentration with the A- and B-atoms diffusing in the opposite direction. The flux of B-atoms is larger than that of A, leading to component segregation and phase transformation

An interesting feature is the enhanced segregation along the phase interfaces, as evident in Fig. 6. We measure the concentration distribution evolution along two

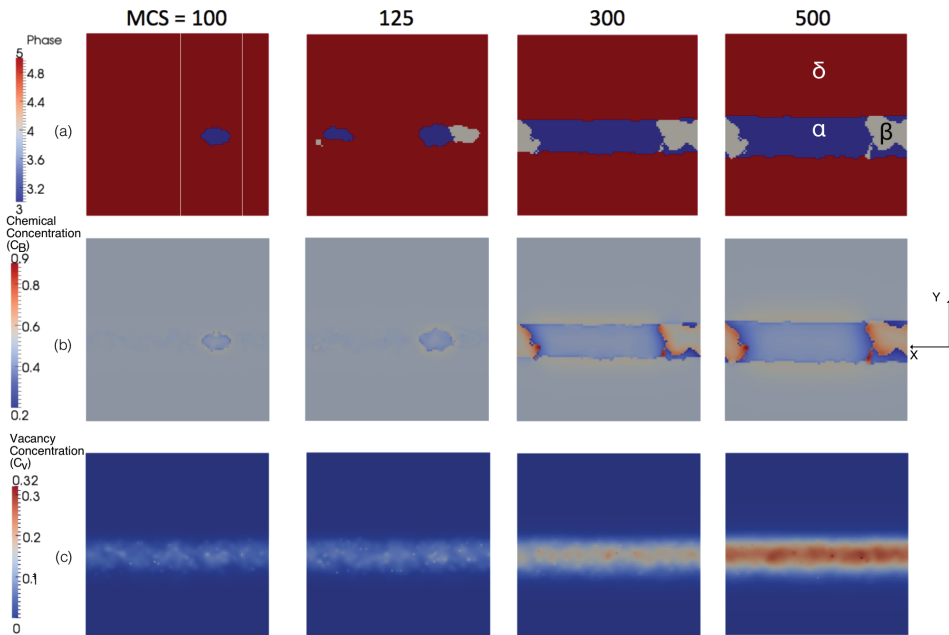


Figure 5: Evolution of the chemical and vacancy compositional, and phase fields as the material with a distribution peaking at the center. The creation and diffusion of the vacancies leads to chemical segregation and phase transformations, where red is the δ phase, blue is the α phase and white is the β phase. (The white vertical lines on the top left image are referenced in Figure 6.)

different paths through the simulation in Fig. 5. Along one line, a single phase nucleates and grows, Fig. 6(a). Along the other line two phases, nucleate and grow, Figure 6(b). The vacancy concentration profiles for both cases are very similar as would be expected, however, the B-concentration profiles are different. Initially, the two paths follow a similar compositional evolution with components A and B segregating similarly until nucleation starts taking place. After 125 MCS, we start seeing an obvious deviation between the composition evolutions. For the two-phase case, Figure 6(b), several concentration “sinks” at the $\alpha - \beta$ interface start forming where each peak corresponds to the equilibrium concentration for the respective phases. For clarity, let us look at the C_B distribution at 125 MCS. Going along the path from top (left) to bottom (right), we see the following features:

- Slight increase in the concentration: this is due to the α phase moving to a lower concentration

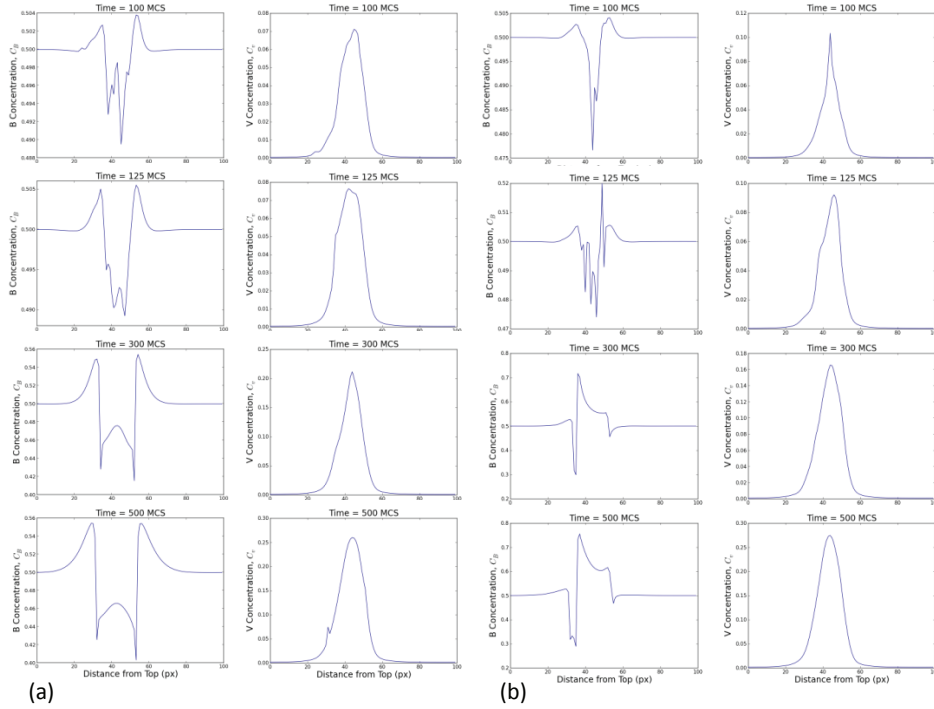


Figure 6: Chemical and vacancy concentration distribution along two different paths (drawn on Figure 5). We look at the concentration evolution along paths that include: a) nucleation of a single phase (left line on Figure 5, α -phase), and b) nucleation of a two phases (right line on Figure 5, α - and β - phases).

- Sharp decrease: boundary of the nucleated α phase at the equilibrium concentration
- Sharp increase: boundary of the nucleated β phase at the equilibrium concentration
- Gradual decrease/increase: bulk of the β phase slowly moves to the equilibrium concentration. The flux within the nucleated phase is much slower than at the interface

The single-phase B-concentration evolution shows peaks corresponding the α equilibrium concentration along the interface with the initially stable AB phase. This is a much simpler distribution, but with similar behavior of reaching the equilibrium concentration almost immediately after nucleation and a slower transition within

the bulk of the phase.

We should note that the concentration at the interfaces reaches equilibrium at a much faster rate than within the phase's bulk due to the larger difference in the chemical potential between different phases, i.e., larger driving force leads to a faster flux ($J \propto F \propto \nabla\mu$).

4 Summary

The model presented in this work has been shown to simulate RIS in a two-component, three-phase system. Radiation damage was introduced as the energy associated with irradiation defects, namely vacancies. Differential diffusion occurred as the two components diffused at very different rates thus allowing the components to separate. Phase transformation occurred when the α or β phase had a lower free energy than the δ phase for the local composition and radiation damage. As multiple phases were being simulated with different free energy curves, the use of the complete chemical potential definition was necessary to accurately capture the thermodynamics of all the phases. This model was able to simulate a chemical depletion/enrichment behavior leading to the nucleation and growth of distinct phases. The model captured the detailed variations in composition, structure and phases at the nano-scale. The model demonstrates that differential diffusivity is sufficient to lead to RIS.

Acknowledgement: Sandia National Laboratories is a multi-program laboratory managed and operated by Sandia Corporation, a wholly owned subsidiary of Lockheed Martin Corporation, for the U.S. Department of Energy's National Nuclear Security Administration under contract DE-AC04-94AL85000.

References

Bradley, R. M.; Harper, J. M. E. (1988): Theory of ripple topography induced by ion bombardment. *J. Vac. Sci. Technol. A*, vol. 6, pp. 2390–2395.

Bruemmer, S. M.; Simonen, E. P.; Scott, P. M.; Andresen, P. L.; Was, G. S.; Nelson, L. J. (1999): Radiation-induced material changes and susceptibility to intergranular failure of light-water-reactor core internals. *J. Nucl. Mats.*, vol. 274, pp. 299–314.

Hernández-Rivera, E.; Tikare, V.; Wang, L. (2013): Simulation of Radiation-Induced Segregation by the Hybrid Potts-Phase Field Model. *Thermec Proceedings*, accepted

Hobler, G.; Simionescu, A.; Palmetshofer, L.; Tain, C.; Stinger, G. (1995):

Boron channeling implantations in silicon: Modeling of electronic stopping and damage accumulation. *J. Appl. Phys.*, vol. 77, pp. 3697–3703.

Holm, E. A.; Battaile, C. C. (2001): The Computer Simulation of Microstructural Evolution. *JOM*, vol. 53, pp. 20–23.

Homer, E. R.; Tikare, V.; Holm, E. A. (2013): Hybrid Potts–phase field model for coupled microstructural–compositional evolution. *Comput. Mat. Sci.*, vol. 69, pp. 414–423.

Le Roy, S.; Barthel, E.; Brun, N.; Lelarge, A.; Sondergard, S. (2009): Self-sustained etch masking: A general concept to initiate the formation of nanopatterns during ion erosion. *J. Appl. Phys.*, vol. 106, pp. 094308 1–5.

Lupis, C. H. P. (1983): *Chemical Thermodynamic of Materials*. first ed., Elsevier Science, New York.

Madi, C. S.; Anzenberg, E.; Ludwig, Jr., K. F.; Aziz, M. J. (2011): Mass Redistribution Causes the Structural Richness of Ion-Irradiated Surfaces. *Phys. Rev. Lett.*, vol. 106, pp. 066101 1–4.

Okamoto, P. R.; Rehn, L. E. (1979): Radiation–induced segregation in binary and ternary alloys. *J. Nucl. Mats.*, vol. 83, pp. 2–23.

Perez–Bergquist, A. G.; Li, K. D.; Zhang, Y.; Wang, L. (2010): Ion irradiation–induced bimodal surface morphology changes in InSb. *Nanotech.*, vol. 21, pp. 325602 1–6.

Perez–Bergquist, A. G.; Sun, K.; Wang, L.; Zhang, Y. (2009): Formation of GaSb core–shell nanofibers by a thermally induced phase decomposition process. *J. Mats. Res.*, vol. 24, pp. 2286–2292.

Was, G. (2007): *Fundamentals of Radiation Materials Science: Metals and Alloys*. first ed., Springer, New York.

Wei, Q.; Lian, J.; Lu, W.; Wang, L. (2008): Highly Ordered Ga Nanodroplets on a GaAs Surface Formed by a Focused Ion Beam. *Phys. Rev. Lett.*, vol. 100, pp. 076103 1–4.

Wei, Q.; Lian, J.; Boatner, L. A.; Wang, L.; Ewing, R. C. (2009): Propagation of ripples on pyrochlore induced by ion beam bombardment. *Phys. Rev. B*, vol. 80, pp. 085413 1–8.

Wiedersich, H.; Okamoto, P. R.; Lam, N. Q. (1979): A Theory of Radiation–Induced Segregation in Concentrated Alloys. *J. Nucl. Mats.*, vol. 83, pp. 98–108.

Ziegler, J.; Ziegler, M.; Biersack, J. (2008): *SRIM: The Stopping and Range of Ions in Matter*. version 2008.03, LuLu, Morrisville NC.

